Hindawi
Scientific Programming
Volume 2022, Article ID 5747974, 13 pages
https://doi.org/10.1155/2022/5747974

*Research Article*

# Quantitative Inversion Model Design of Mine Water Characteristic Ions Based on Hyperspectral Technology

**Yunbo Li** [1,2]

[1]*State Key Laboratory of the Gas Disaster Detecting, Preventing and Emergency Controlling, Chongqing 400037, China*
[2]*China Coal Technology and Engineering Group Chongqing Research Institute, Chongqing 400039, China*

Correspondence should be addressed to Yunbo Li; liyunbo@cqccteg.com

Received 4 June 2022; Revised 7 July 2022; Accepted 11 July 2022; Published 1 August 2022

Academic Editor: Lianhui Li



In view of the problems of low measurement accuracy and repeated calibration during the use of coal mine water quality analysis, the hyperspectral reflection noncontact measurement technology was proposed to solve the existing problems. KCl, NaCl, pH, $NaHCO_3$, and $CaCl_2$were used to indicate the characteristic ion information of $Na^+$, $K^+$, $Ca^{2+}$, $Cl^-$, $HCO_3^-$, and pH mine water in the laboratory, and 2220 spectral data were obtained by spectral determination. Savitzky–Golay convolution smoothing was used to smooth and denoise the original spectral data of each ion, and the relationship between the spectrum and the concentration of each reagent was obvious after smoothing and denoising pretreatment. The principal component regression method was used to build the inversion model of each ion content, and through the modeling study, the prediction set of KCl was found: the coefficient R^2 reaches 0.907, RPD is up to 2.7; the prediction set of NaCl was found: the coefficient R^2 reaches 0.957, RPD is up to 3.1; the PH prediction set was found: the coefficient R^2 reaches 0.785, RPD is up to 2.1; the prediction set of NaHCO3 was found: the coefficient R^2 reaches 0.137, RPD is up to 1.2; the prediction set of CaCl2 was found: the coefficient R^2 reaches 0.622, and RPD is up to 1.7. The results show that the hyperspectral method can play a better role in the extraction of $K^+$, $Cl^-$, $Na^+$, $Ca^{2+}$, and pH. It is difficult to extract $HCO_3^-$ ions.

## 1. Introduction

Water hazard is one of the main threats to the safety of coal mine production, which causes serious loss of life and property. The prevention and control of water disaster in coal mines take water filling channel, water filling source, and water filling intensity as the main objects and take exploration, prevention, blocking, dredging, drainage, interception, and monitoring as the main means. Water samples are collected after water inrush or water gushing occurs in a mine, and the source of the water inrush or water gushing is judged by using the chemical composition of the water. It is a method widely used by technicians of geological survey and water control engineering in coal mines.

In foreign countries, the rock mass structure of coal seam floor and the prevention and drainage technology have been studied in depth, and a lot of experience has been accumulated in the mechanism of water inrush and the identification of water hazards. In the book Hydrogeochemistry written by Clevers et al., the application of groundwater pollution and chemical evaluation in hydrochemical analysis is systematically discussed from the perspective of hydrogeochemistry [1–4]. Clevers et al. obtained it by using the 3D edge detection seismic attribute method [1–4]. Clevers et al. used hydrological observation and a tracer test to test the effect of the tunnel drainage system [1–4]. However, there is little research work on the application of mine water chemistry and the identification of mine water inrush sources.

The main method of discriminating the source of water inrush in coal mines in China is the conventional hydrochemical discrimination method. By measuring the eight most widely distributed ions in groundwater, such as $Ca^{2+}$, $Mg^{2+}$, $K^+$, $Na^+$, $CO3^{2-}$, $HCO_3^-$, $SO4^{2-}$, and $Cl^-$. Its concentration accounts for more than 90% of the total ion concentration in groundwater, as well as the characteristic ion ratio, hardness, temperature, TDS index, and pH value [5–10]. The mine water chemical data of Taoyuan Coal Mine

was processed by using Piper's three-line diagram [5–7]. The hydrochemical characteristics of each aquifer in the Xuzhou mining area were introduced [8, 9]. Conventional hydrochemical methods were used to carry out hydrogeochemical analysis of underground aquifers in a mine in Xuzhou [10–12]. The conventional hydrochemistry of four water-bearing subsystems in Yaoqiao Mine, Xuzhou, was studied [13–16]. A systematic study on the hydrochemical characteristics of groundwater in the Ordovician karst aquifer in the middle part of the Taihang Mountains was made [17–20]. The Chongqing Research Institute of China Coal Science and Technology Group, Beijing Huaan Auto, and Wuhan Dida Huarui have carried out relevant research on water quality analysis technology and equipment and have applied it in various coal mine groups [21–29].

However, there are still some problems in the current underground ion electrode monitoring, such as inaccurate measurement and repeated calibration during use, which cannot meet the needs of online identification of water sources. It is urgent to develop a new type of online water quality analysis sensors.

## 2. Hyperspectral Experimental Determination of Common Ions in Mine Water

The purpose of the experimental test is to find the hyperspectral characteristic band of the liquid related to the coal mine. The experimental spectral acquisition equipment is a self-made spectral probe, and the experimental measurement process is composed of three parts of spectrometer calibration, standard solution production, spectral measurement, and accuracy evaluation [30].

Five reagents, NaCl, KCl, $CaCl_2$, $NaHCO_3$, and pH buffer, were measured to indicate $Na^+$, $K^+$, $Ca^{2+}$, $Cl^-$, $HCO_3^-$, and pH ion information, wherein the potassium ion and the chloride ion are indicated by KCl standard solution for a set of data (see Table 1 for details) [31–33]. Before measurement, the mother liquor is diluted with deionized water, and according to the test requirements, the sodium ion, potassium ion, chloride ion, and calcium ion dilution levels are 10, 50, 100, 500, 1000, and 10000 mg/L, the carbonate dilution levels are 0.44, 2.2, 4.4, 22, 44, and 440 mg/L, and the pH dilution levels are 4, 6.86, and 9.18. According to the order of KCl, NaCl, pH, $NaHCO_3$, $CaCl_2$, pure water, empty barrel, and green plants, 8 kinds of targets were measured, totaling 2220 hyperspectral data. Figure 1 shows the number of spectra of various standard solutions.

## 3. Ion Hyperspectral Data Preprocessing and Sensitive Band Selection

We carry out spectral quality evaluation on all obtained spectral data and select qualified spectral data [34–37]. At the same time, due to the influence of the external environment, there are many "burr" noises on the spectral curve, so it is necessary to reduce the noise on the spectral curve after smoothing and filtering. In this study, Savitzky–Golay convolution smoothing was used to smooth and denoise the original spectral data of each ion. The value of the spectrum after Savitzky–Golay smoothing at wavelength I is

$$x_{i,\text{Savitzky–Golay}} = \frac{\sum_{j=-m}^{m} c_j x_{i+j}}{N}. \quad (1)$$

In the formula, $x_{i,\text{Savitzky–Golay}}$ is the smoothed value at the wavelength $I$, $x$ is the value before smoothing, $m$ is the number of smoothing windows on the wavelength side, $N$ is the normalization index, and $\sum_{j=-m}^{m} c_j$ is the smoothing coefficient, which can be obtained by polynomial fitting.

After smooth denoising pretreatment, the relationship between the spectrum and the concentration of each reagent is evident. Compared with the spectral data of "pure water + gradient" concentration, KCl, NaCl, pH, $NaHCO_3$, and $CaCl_2$ have obvious sensitive bands and rules. The higher the concentration of KCl, NaCl, and $CaCl_2$, the lower the overall reflectivity, which should be the mechanism under the action of $Cl^-$. The pH data show that the reflectivity of pure water and acidic liquid is in the middle. The reflectivity of neutral liquid is low and that of alkaline liquid is the highest. As a whole, the higher the concentration of $NaHCO_3$, the higher the reflectivity. Figure 2 shows the comparison of the KCl, NaCl, and pH spectral data before and after denoising, while Figure 3 shows the comparison of the spectral data of $NaHCO_3$, $CaCl_2$, and pure water before and after denoising.

## 4. Establishment of the Quantitative Inversion Prediction Model for Ion Hyperspectral Data

The mine water is a complex system composed of various chemical ions in the water. In this study, the principal component regression (PCR) method is used to establish the quantitative inversion model, which is based on principal component analysis (PCA) [38–46]. PCA is a multiple collinearity regression analysis method. The principle is that after the multicollinearity in the regression model is eliminated by the principal component analysis method, the principal component variables are used as independent variables for regression analysis, and then, the original variables are substituted back into the new model according to the score coefficient matrix.

The basic steps of PCA are as follows:

(1) The aim is to acquire a principal component of independent variable data through principal component analysis and select a principal component subset through standardized classification.

(2) The principal component obtained in step (1) is used as a new independent variable, and an estimated regression coefficient vector is obtained through linear regression analysis (the dimension is equal to the number of the selected principal components).

(3) We transform the regression coefficient vector into the proportion of the actual independent variables and use the selected PCA load (corresponding to the eigenvector of the selected principal component) to

Table 1: Standard solutions of five ions.

| No<br>Reagent | Sodium ion<br>NaCl | Potassium ion<br>KCl | Chloride ion | Calcium ion<br>$CaCl_2$ | Carbonate<br>$NaHCO_3$ | pH<br>pH buffer |
|---|---|---|---|---|---|---|
| 1 | 10 | 10 | 10 | 10 | 0.44 | 4 |
| 2 | 50 | 50 | 50 | 50 | 2.2 | 6.86 |
| 3 | 100 | 100 | 100 | 100 | 4.4 | 9.18 |
| 4 | 500 | 500 | 500 | 500 | 22 | — |
| 5 | 1000 | 1000 | 1000 | 1000 | 44 | — |
| 6 | 10000 | 10000 | 10000 | 10000 | 440 | — |

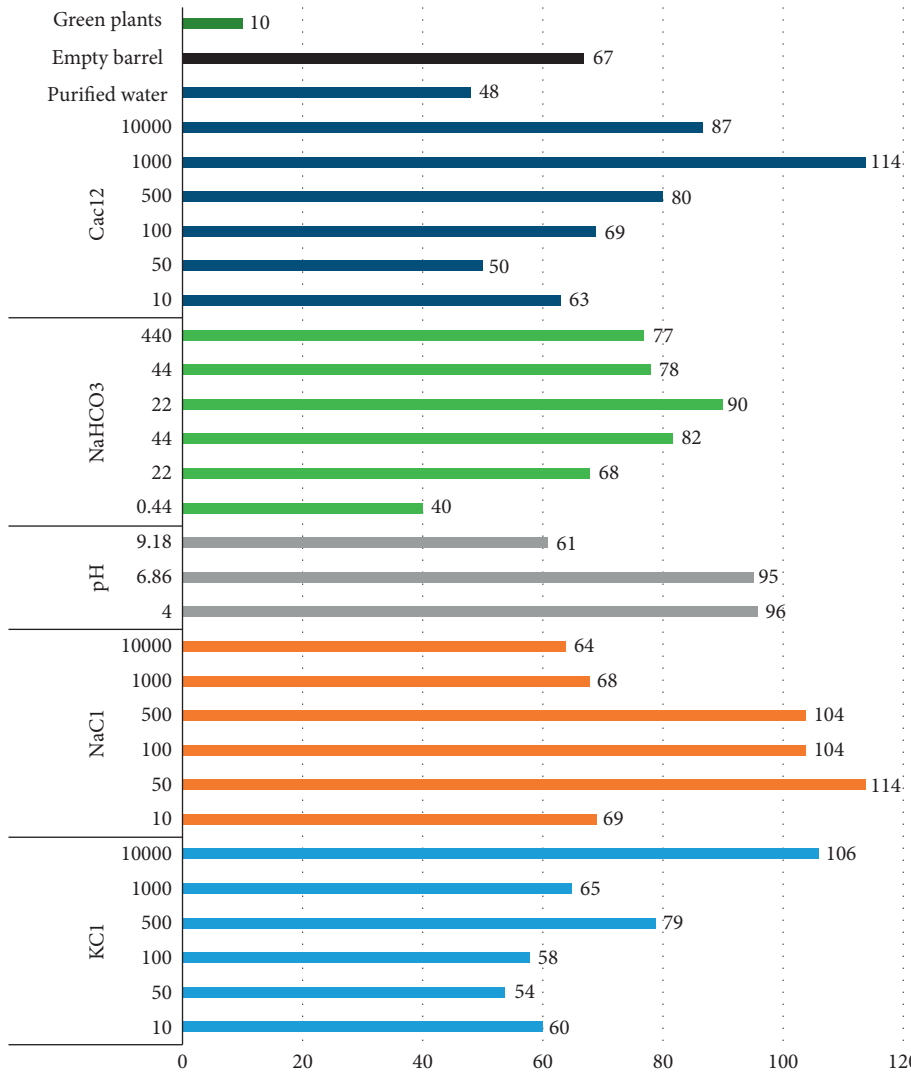


Figure 1: The number of spectra of various standard solutions.

obtain the final PCR estimator (dimension equal to the total number of independent variables) for estimating the regression coefficients.

For model evaluation, cross-validation was used to evaluate the model, and determination coefficients ($R^2$ and root mean of squared error (RMSE) were selected. The RMSE and relative percent deviation (RPD) were used as evaluation indexes. When the $R^2$ value of the calculated validation set is closer to 1, the RMSE value is lower, and when the RPD value is closer to 2, the model is more stable, the accuracy is higher, and the model is better. When $R^2$ is less than 0.50 and RPD is less than 1.40, the estimation ability of the model to the sample is poor, and the model is not available; $0.50 < R^2 < 0.75$ and $1.40 < \text{RPD} < 2.00$, the estimation ability of the model to the sample is improved, but only rough estimation can be made, and the model is available. When $R^2 > 0.75$ and $\text{RPD} > 2.00$, the model accuracy is high, the model is good, and the calculation formula is

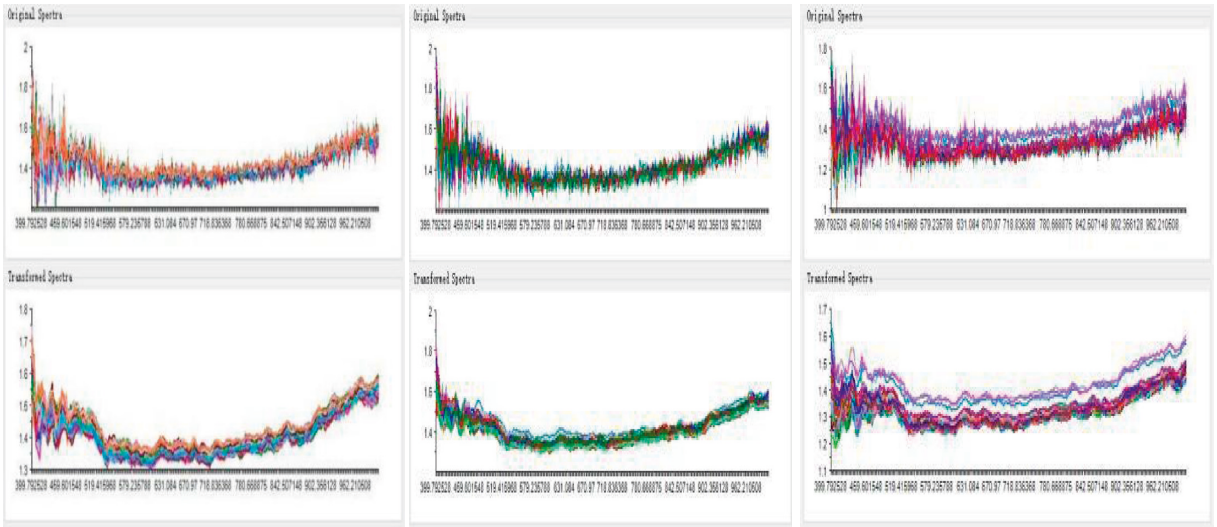


Figure 2: Comparison of the KCl, NaCl, and pH spectral data before and after denoising.

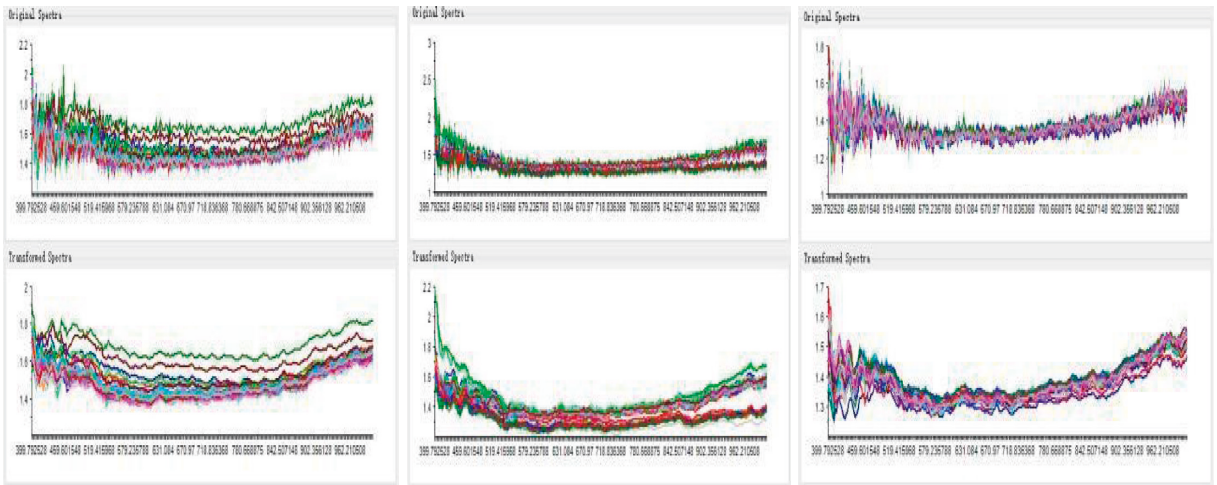


Figure 3: Comparison of the spectral data of $NaHCO_3$, $CaCl_2$, and pure water before and after denoising.

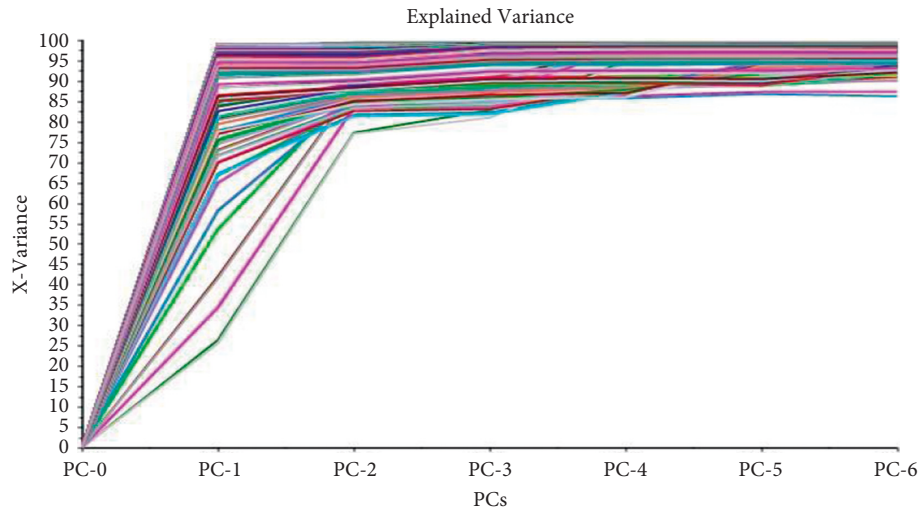


Figure 4: KCl principal component results.

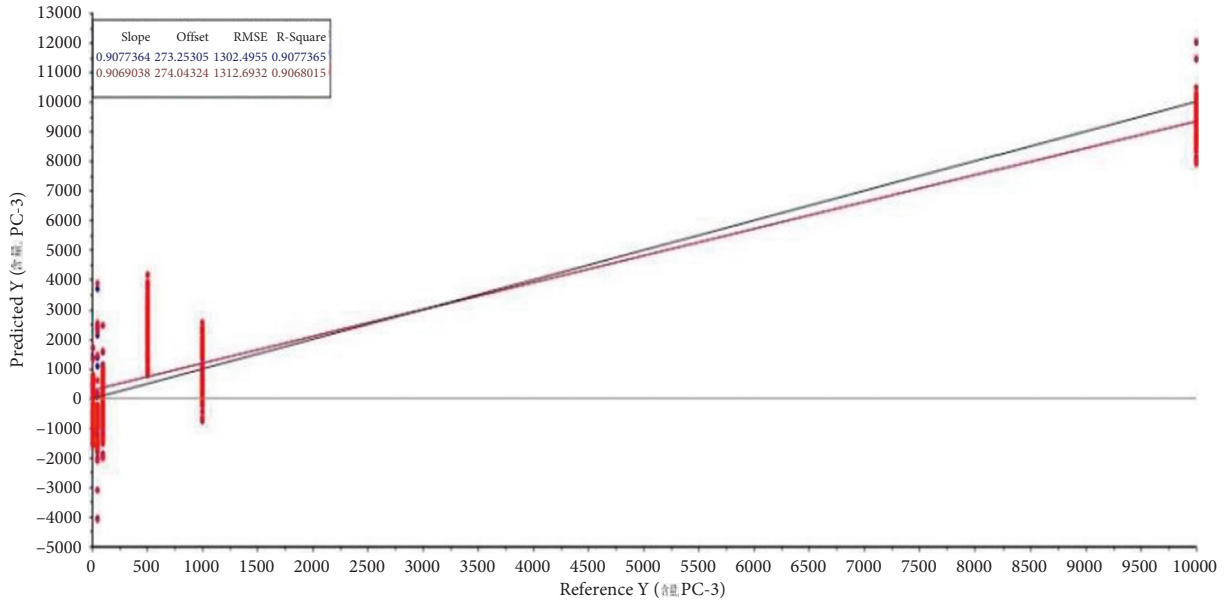


Figure 5: Comparison between the KCl actual measurement set and prediction sets.

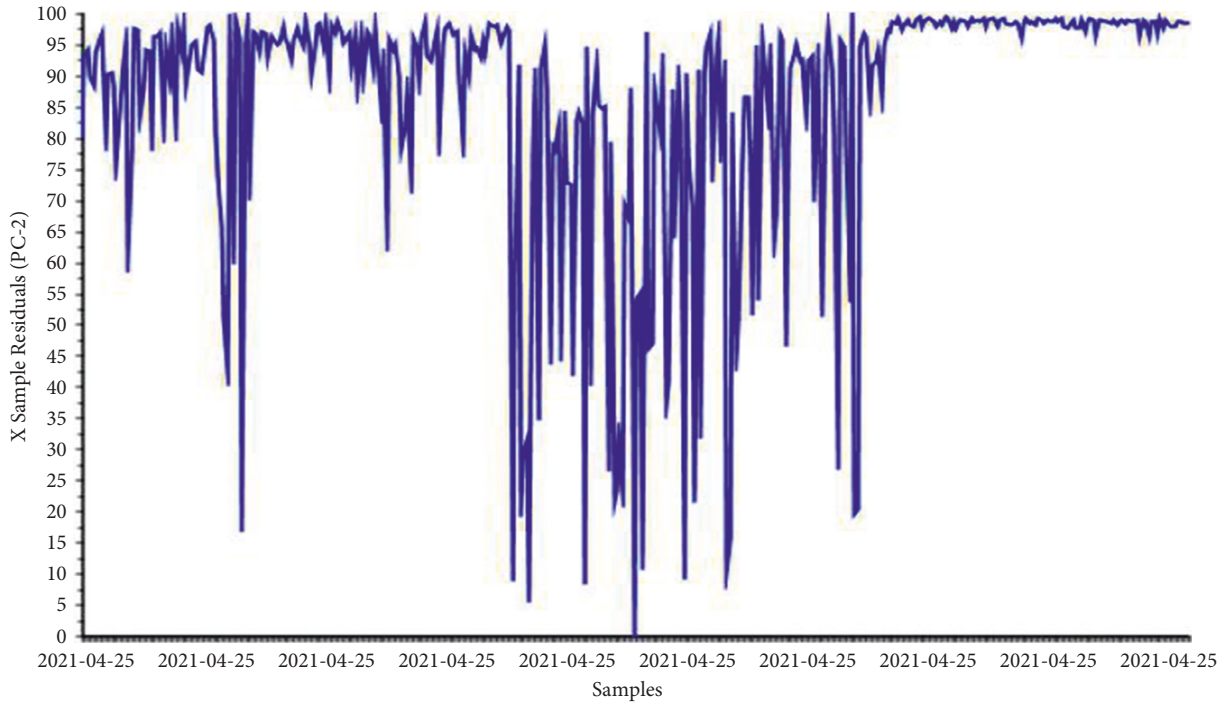


Figure 6: The role of sample points in the calculation of KCl content.

$$R^2 = 1 - \frac{\sum_{i=1}^{n} \left(y_i - y^{\Delta}\right)^2}{\sum_{i=1}^{n} \left(y_i - y^{-}\right)^2}, \tag{2}$$

$$\text{RMSE} = \sqrt{\frac{1}{n} \sum_{i=1}^{n} \left(y_i - y_i^{\Delta}\right)^2}, \tag{3}$$

$$\text{RPD} = \frac{SD}{\text{RMSE}}. \tag{4}$$

In the formula, $y_i$ represents the measured value of the sample I, $y_i^{\Delta}$ represents the predicted value of the sample I, $y^{-}$ represents the mean of all samples, $n$ is the number of samples, and SD is the standard deviation of the measured values of the validation set samples.

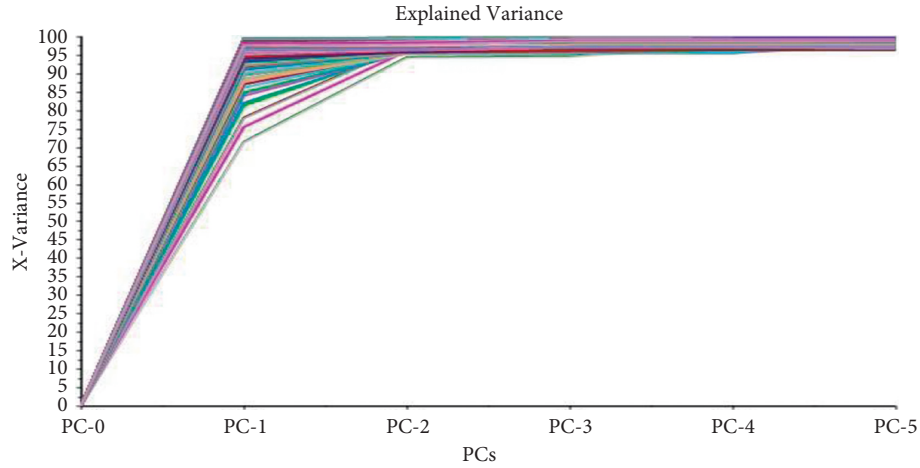


Figure 7: NaCl principal component results.

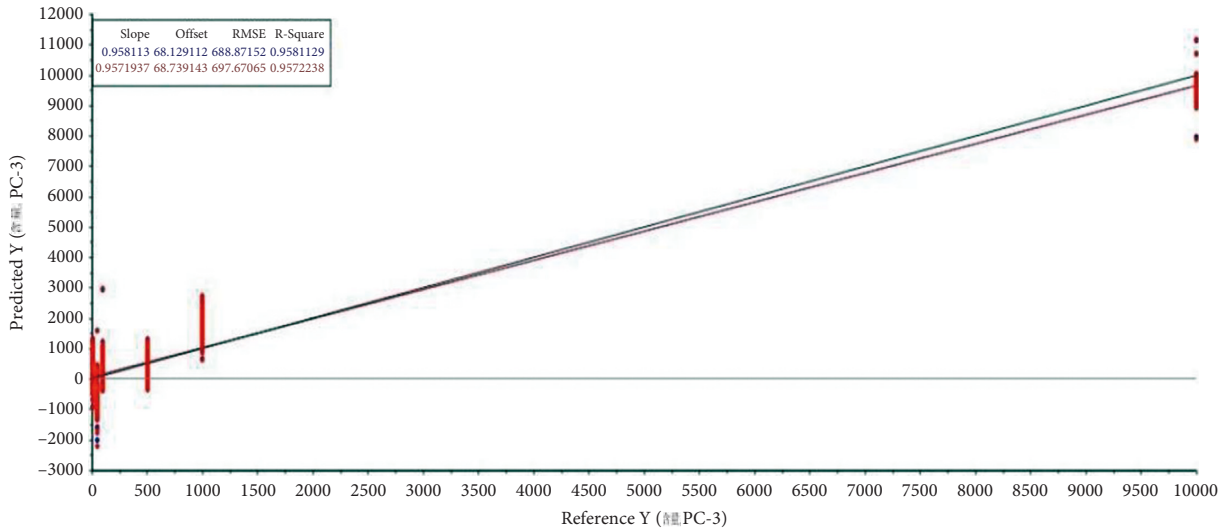


Figure 8: Comparison between measured and predicted NaCl sets.

*4.1. KCl Content Spectral Prediction Modeling.* 382 standard solution spectral data were selected, the largest 7 principal components were selected, and the weights were set equally [47–51]. CV prediction detection, cross-validation, and the principal component analysis model were established when the proportion of the validation set and modeling set was 0.70. The first three principal components can represent more than 80% of the content information. In the modeling set, the coefficient reaches R2 which reaches 0.908, and in the prediction set, the coefficient reaches R2 which reaches 0.907, and RPD is up to 2.7. In the process of computational modeling, the importance of all sample points and the samples collected in the middle section play a greater role. Figure 4 shows the KCl principal component results, Figure 5 shows the comparison between the KCl actual measurement set and prediction sets, and Figure 6 shows the role of sample points in the calculation of KCl content.

*4.2. NaCl Content Spectral Prediction Modeling.* Three hundred and ninety-nine standard solution spectral data were selected, the largest seven principal components were selected, and the weights were set equally [47–51]. CV prediction detection, cross-validation, and the principal component analysis model were established when the proportion of the validation set and the modeling set was 0.70. The first three principal components can represent more than 90% of the content information. In the modeling set, the coefficient reaches R2 which reaches 0.958, and in the prediction set, the coefficient reaches R2 which reaches 0.957, and RPD is up to 3.1. In the process of computational modeling, the importance of all sample points and the samples collected in the middle section play a greater role. Figure 7 shows the NaCl principal component results, Figure 8 shows the comparison between measured and predicted NaCl sets, and Figure 9 shows the role of sample points in the calculation of NaCl content.

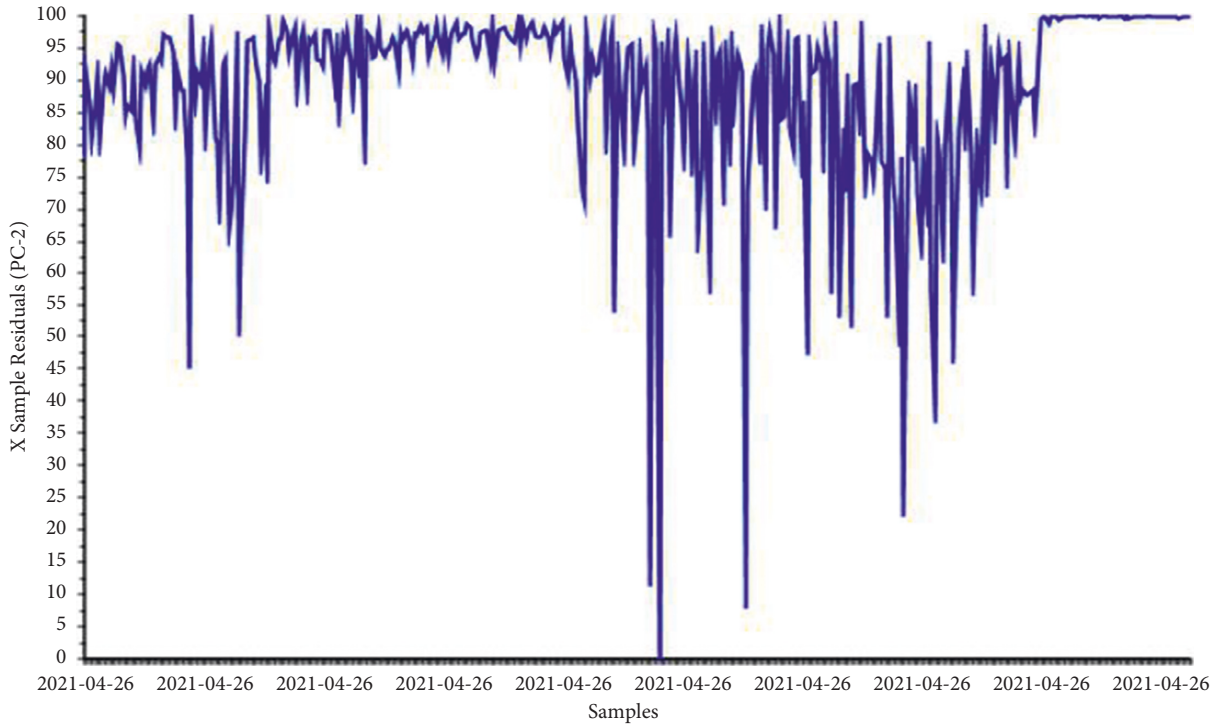


Figure 9: The role of sample points in the calculation of NaCl content.

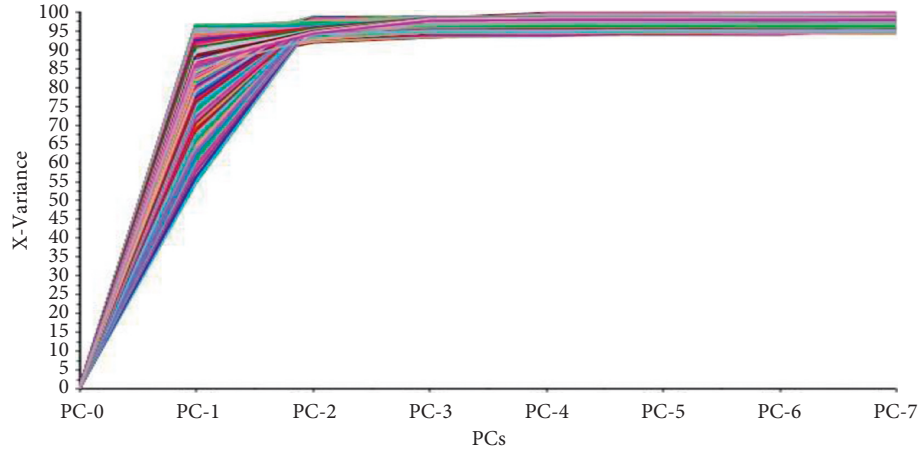


Figure 10: pH principal component results.

*4.3. pH Content Spectral Prediction Modeling.* 240 spectral data of standard solution were selected, the largest 7 principal components were selected, and the weights were set equally [47–51]. CV prediction detection, cross-validation, and the principal component analysis model were established when the proportion of the validation set and the modeling set was 0.70. The first three principal components can represent more than 85% of the content information. In the modeling set, the coefficient reaches R2 which reaches 0.791, and in the prediction set, the coefficient reaches R2 which reaches 0.785, and RPD is up to 2.1. In the process of calculation and modeling, the importance of all sample points and the samples collected in the previous section play a greater role. Figure 10 shows the pH principal component results, Figure 11 shows the comparison between measured and predicted pH sets, and Figure 12 shows the role of sample points in the calculation of pH content.

*4.4. $NaHCO_3$ Content Spectral Prediction Modeling.* 404 standard solution spectral data were selected, the largest 7 principal components were selected, and the weights were set equally [47–51]. CV prediction detection, cross-validation, and the principal component analysis model were established when the proportion of the validation set and the modeling set was 0.70. The first three principal

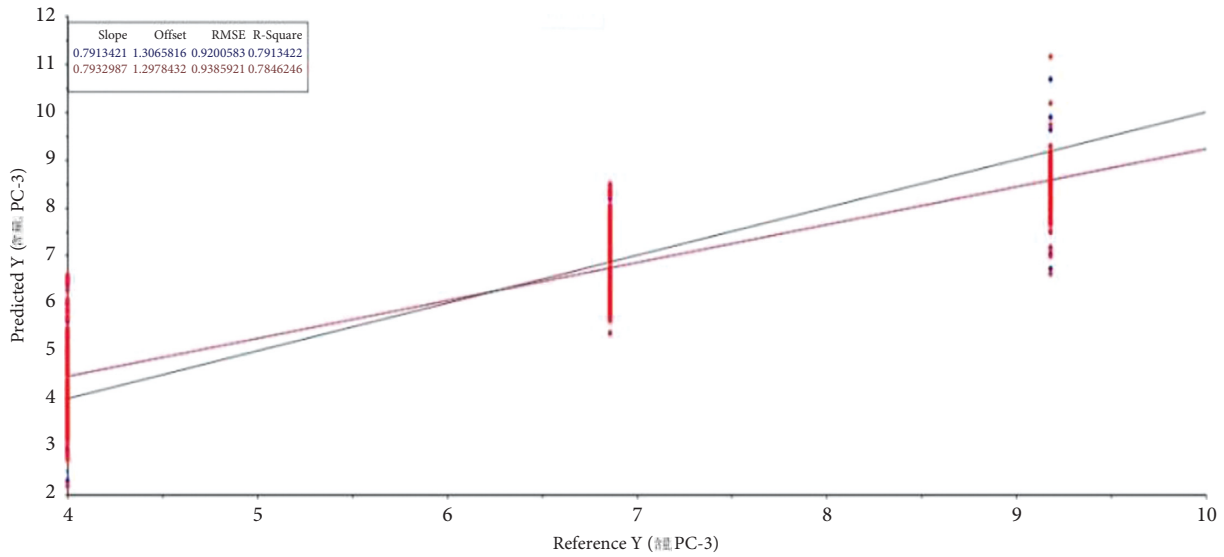


Figure 11: Comparison between measured and predicted pH sets.

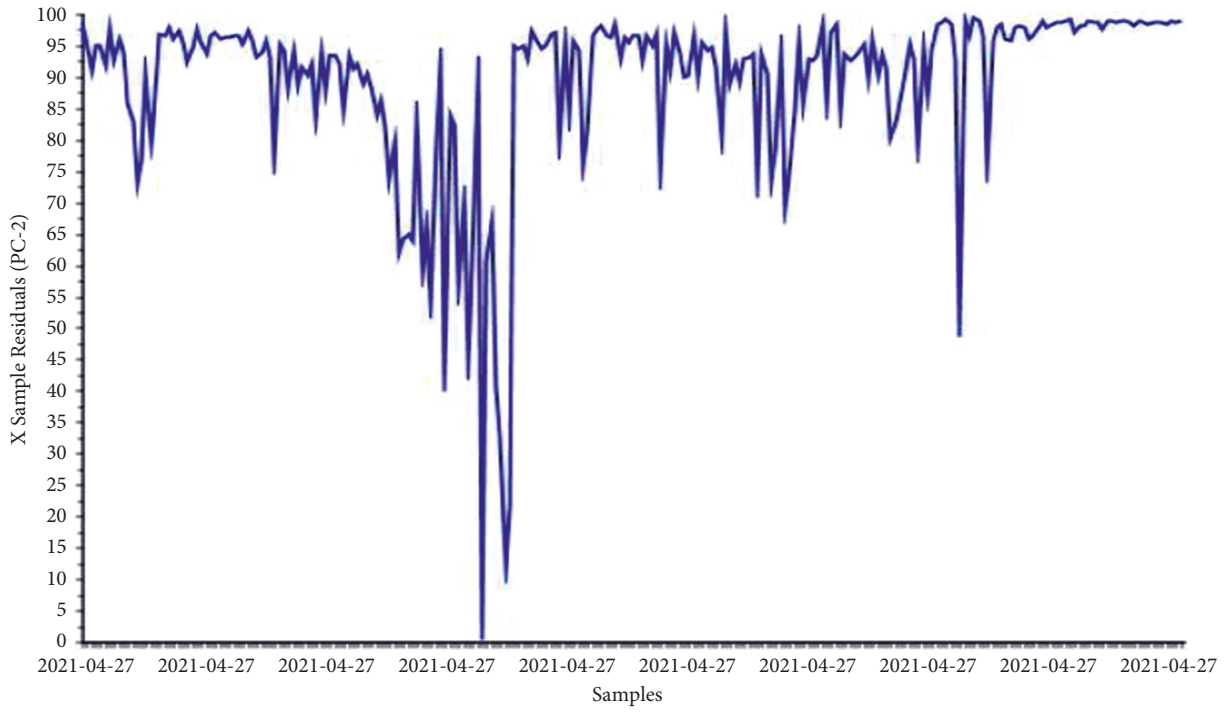


Figure 12: The role of sample points in the calculation of pH content.

components can represent more than 75% of the content information. In the modeling set, the coefficient reaches R2 which reaches 0.162, and in the prediction set, the coefficient reaches R2 which reaches 0.137, and RPD is up to 1.2. In the process of computational modeling, the importance of all sample points and the samples collected in the middle and back end play a greater role. Figure 13 shows the $NaHCO_3$ principal component results, Figure 14 shows the comparison between measured and predicted $NaHCO_3$ sets, and Figure 15 shows the role of sample points in the calculation of $NaHCO_3$ content.

*4.5. $CaCl_2$ Content Spectrum Prediction Modeling.* Four hundred and seventeen standard solution spectral data were selected, the largest seven principal components were selected, and the weights were set equally [47–51]. CV prediction detection, cross-validation, and the principal component analysis model were established when the proportion of the validation set and the modeling set was 0.70. The first three principal components can represent more than 55% of the content information. In the modeling set, the coefficient reaches R2 which reaches 0.630, and in the prediction set, the coefficient reaches R2 which reaches

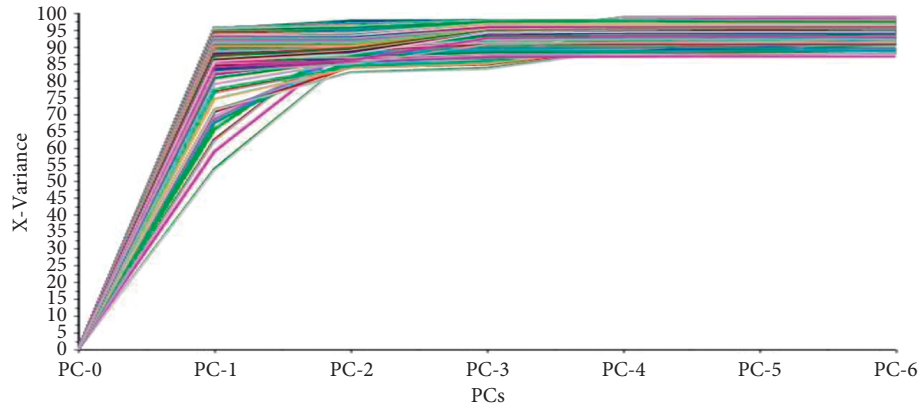


Figure 13: $NaHCO_3$ principal component results.

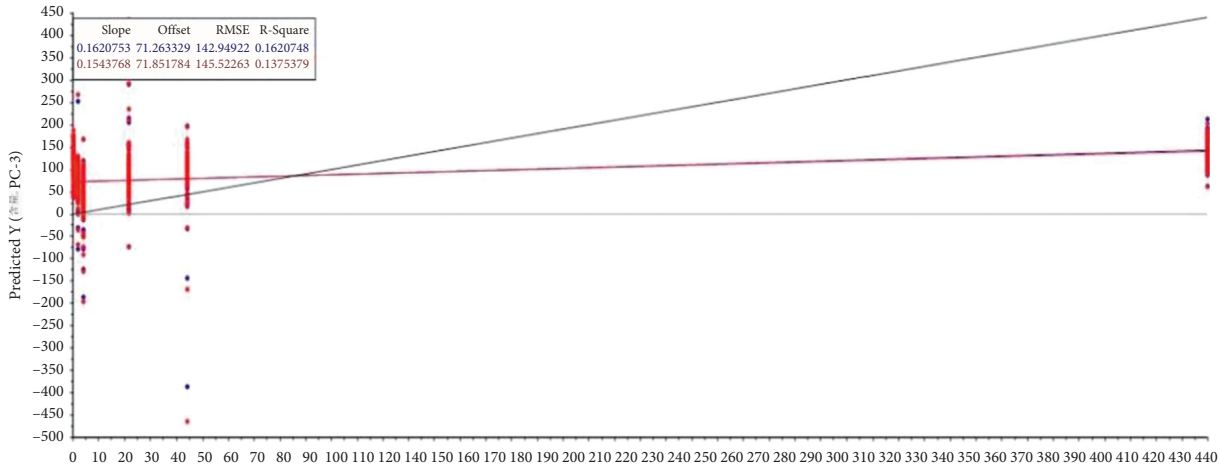


Figure 14: Comparison between measured and predicted $NaHCO_3$ sets.

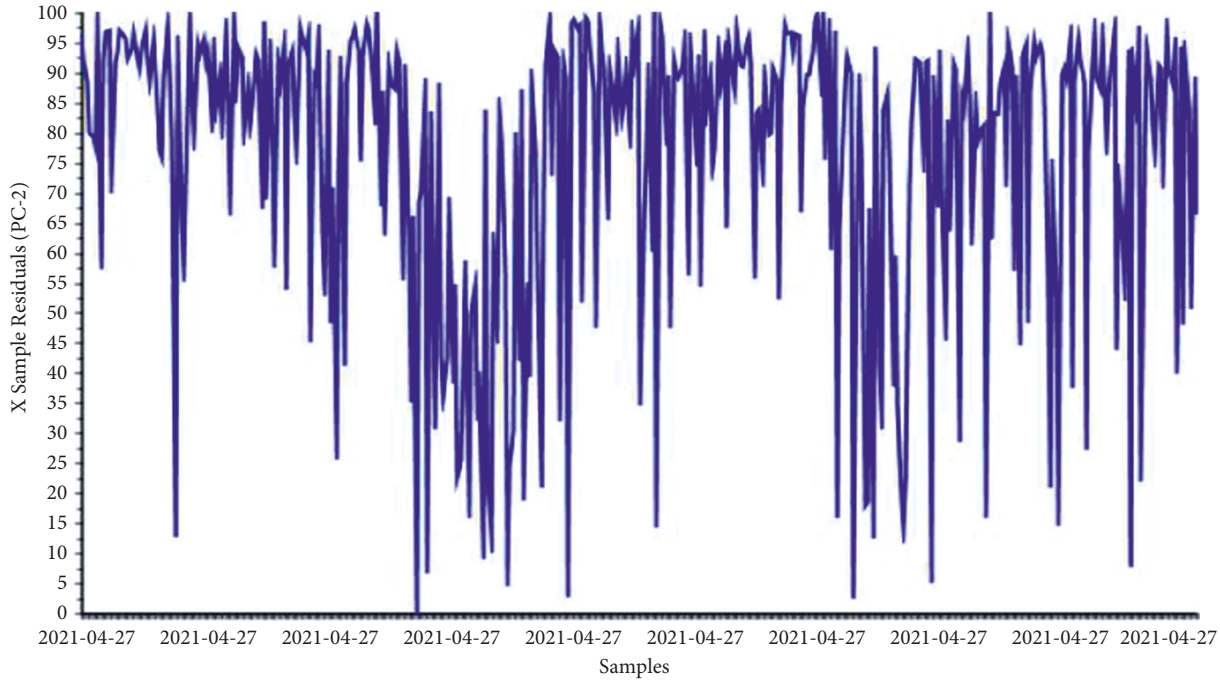


Figure 15: The role of sample points in the calculation of $NaHCO_3$ content.

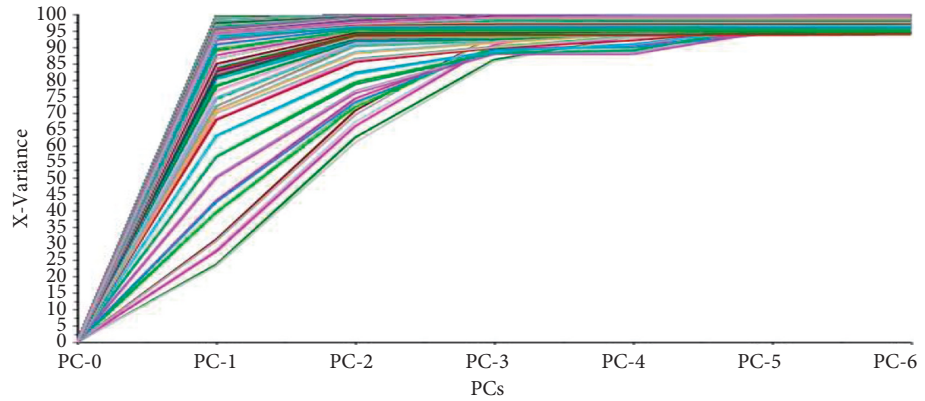


Figure 16: $CaCl_2$ principal component results.

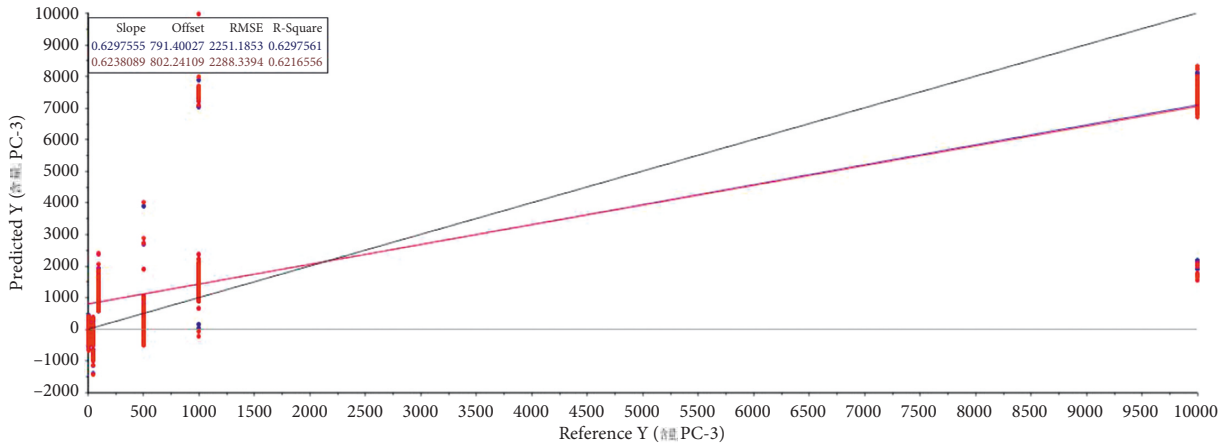


Figure 17: Comparison between measured and predicted sets of $CaCl_2$.

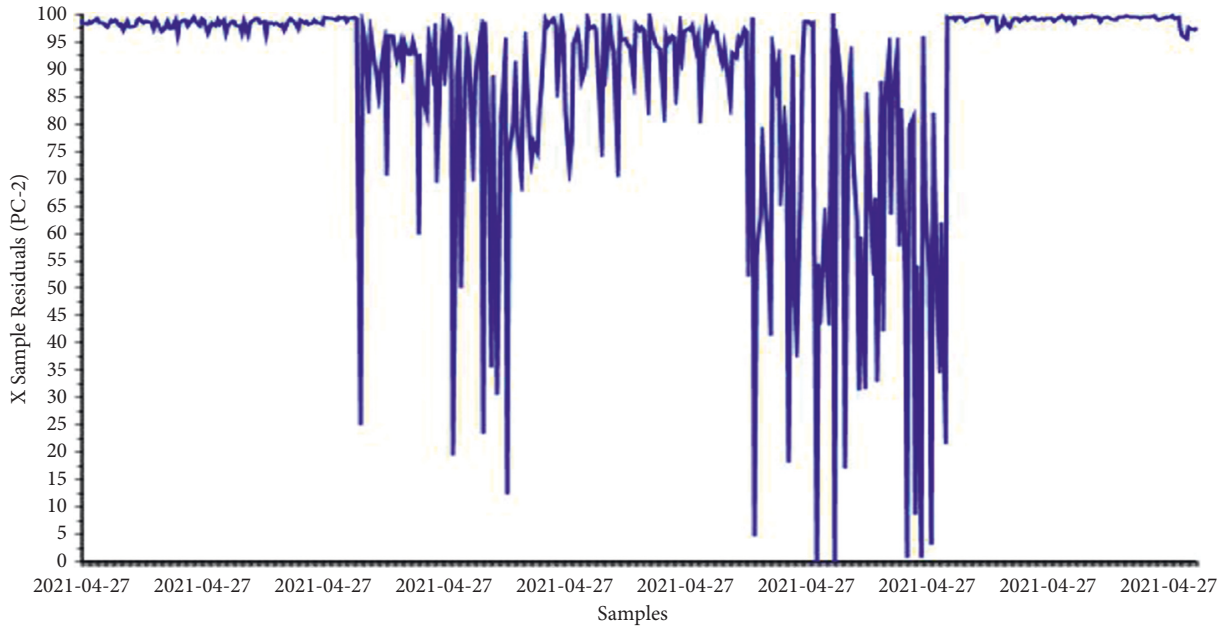


Figure 18: The role of sample points in the calculation of $CaCl_2$ content.

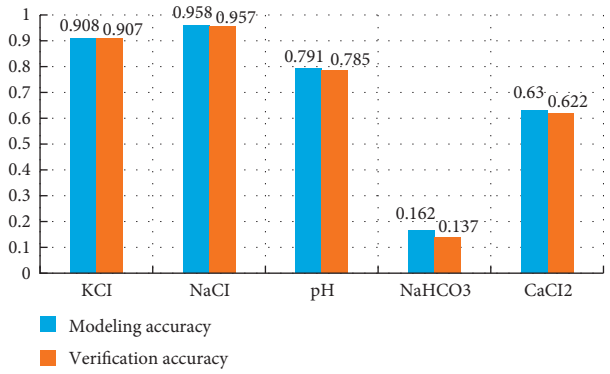


Figure 19: Comparison of extraction accuracy of various ions.

0.622, and RPD is up to 1.7. In the process of computational modeling, the importance of all sample points and the samples collected in the middle section play a greater role. Figure 16 shows the $CaCl_2$ principal component results, Figure 17 shows the comparison between measured and predicted sets of $CaCl_2$, Figure 18 shows the role of sample points in the calculation of $CaCl_2$ content, and Figure 19 shows the comparison of extraction accuracy of various ions.

## 5. Conclusion

Through the spectrum analysis of the characteristic ions of the mine water, the principal component regression method is used to carry out the quantitative inversion modeling of various ions, and the five standard solutions of KCl, NaCl, pH, $NaHCO_3$, and $CaCl_2$ indicate six ions (KCl includes K ions and Cl ions). The extraction precision of KCl and NaCl is higher than 0.9, followed by pH and $CaCl_2$, the precision is more than 0.6. The extraction precision of $HCO_3$ is the lowest, only 0.162. The results show that the hyperspectral method can play a better role in the extraction of $K^+$, $Cl^-$, $Na^+$, $Ca^{2+}$, and pH. It is difficult to extract $HCO_3^-$ ions.

## Data Availability

The dataset can be accessed from the corresponding author upon request.

## Conflicts of Interest

The author declares no conflicts of interest.

## Acknowledgments

The project was supported by the "Thirteenth Five-Year Plan," the Key National R&D Program (Online Dynamic Detection Technology and Equipment of Radio Wave Perspective in Mining Face, 2018YFC0807805).

## References

[1] J. G. P. W. Clevers and L. Kooistra, "Using hyperspectral remote sensing data for Retrieving Canopy chlorophyll andNitrogen content," *Ieee Journal of Selected Topics in Applied Earth Observations and Remote Sensing*, vol. 5, no. 2, pp. 574–583, 2012.

[2] B. Bansod, R. Singh, and R. Thakur, "Analysis of water quality parameters by hyperspectral imaging in Ganges River," *Spatial Information Research*, vol. 26, no. 2, pp. 203–211, 2018.

[3] C. Giardino, V. E. Brando, P. Gege et al., "Imaging Spectrometry of Inland and coastal waters: State of the Art, Achievements and perspectives," *Surveys in Geophysics*, vol. 40, no. 3, pp. 401–429, 2018.

[4] K. Ryan and K Ali, "Application of a partial least-squares regression model to retrieve chlorophyll-a concentrations in coastal waters using hyper-spectral data," *Ocean Science Journal*, vol. 51, no. 2, pp. 209–221, 2016.

[5] W. Liu, Z. Zhao, H. Yuan, C. F. Song, and X. Y Li, "An optimal selection method of samples of calibration set and validation set for spectral multivariate analysis," *Spectroscopy and Spectral Analysis*, vol. 34, no. 4, pp. 947–951, 2014.

[6] X. Peng, W. Gao, and J. Wang, "Inversion of Soil parameters from hyperspectral based on Continuum Removal and partial least squares regression," *Geomatics and Information Science of Wuhan University*, vol. 39, no. 7, pp. 862–866, 2014.

[7] Z. Zhang, H. Wang, A. Karnieli, and J. Chen, "Inversion of Soil Moisture content from Hyperspectra based on ridge regression," *Transactions of the Chinese Society for Agricultural Machinery*, vol. 49, no. 5, pp. 240–248, 2018.

[8] X. Tang, J. Zhou, Na Zhang, and Q. Liu, "Nonlinear Internal model control system based on weighted Regularized Extreme learning machine," *Journal of University of Electronic Science and Technology of China*, vol. 45, no. l, pp. 96–101, 2016.

[9] Y. Zhang and L. I. Mei, "A Novel evaluation model of water quality based on PSO-ELM method," *Environmental Science & Technology*, vol. 39, no. 5, pp. 135–139, 2016.

[10] H. Yao, R. Huang, F. Gan, and Y. Liu, "Principal component analysis of the water quality evaluation in East lake," *Geomatics and Information Science of Wuhan University*, vol. 30, no. 8, pp. 732–735, 2005.

[11] H. Lin and Z. Du, "Some problems in Comprehensive evaluation in the principal component analysis," *Statistical Research*, vol. 30, no. 8, pp. 25–31, 2013.

[12] H. Zou, L. Jiang, and F. Li, "Water quality evaluation method based on principal component analysis," *Mathematics in Practice and Theory*, vol. 20, no. 8, pp. 85–90, 2008.

[13] G. B. Huang, Q. Y. Zhu, and C. K. Siew, "Extreme learning machine: a new learning scheme of feedforward neural networks," in *Proceedings of the 2004 IEEE International Joint Conference on IEEE*, pp. 985–990, IEEE, Budapest, Hungary, July 2004.

[14] M. A. Cho and A. K. Skidmore, "A new technique for extracting the red edge position from hyperspectral data: the linear extrapolation method," *Remote Sensing of Environment*, vol. 101, no. 2, pp. 181–193, 2006.

[15] P. Chen, D. Haboudane, N. Tremblay, J. Wang, P. Vigneault, and B. Li, "New spectral indicator assessing the efficiency of crop nitrogen treatment in corn and wheat," *Remote Sensing of Environment*, vol. 114, no. 9, pp. 1987–1997, 2010.

[16] K. Mcgwire, T. Minor, and L. Fenstermaker, "Hyperspectral Mixture modeling for Quantifying Sparse Vegetation Cover in Arid environments," *Remote Sensing of Environment*, vol. 72, no. 3, pp. 360–374, 2000.

[17] M. A. Vega-Rodríguez, C. J. Pérez, K. Reder, and M. Florke, "A Stage-based Approach to Allocating water quality monitoring Stations based on the WorldQual model: the Jubba river as a Case study," *Science of The Total Environment*, vol. 762, pp. 144–162, 2020.

[18] L. Wei, C. Huang, Z. Wang, Z. Wang, X. Zhou, and L. Cao, "Monitoring of Urban Black-Odor water based on Nemerow index and gradient Boosting Decision tree regression using UAV-Borne hyperspectral imagery," *Remote Sensing*, vol. 11, no. 20, p. 2402, 2019.

[19] K. Drnhfer and N. Oppelt, "Remote sensing for lake research and monitoring C Recent advances," *Ecological Indicators*, vol. 64, pp. 105–122, 2016.

[20] L. Feng, X. Hou, and Y. Zheng, "Monitoring and understanding the water transparency changes of fifty large lakes on the Yangtze Plain based on long-term MODIS observations," *Remote Sensing of Environment*, vol. 221, pp. 675–686, 2019.

[21] F. Baltacı, A. Kübra Onur, and S. Tahmiscioğlu, "Water quality monitoring studies of Turkey with present and probable future constraints and opportunities," *Desalination*, vol. 226, no. 1–3, pp. 321–327, 2008.

[22] M. M. Squires, L. F. W. Lesack, and D. Huebert, "The influence of water transparency on the distribution and abundance of macrophytes among lakes of the Mackenzie Delta, Western Canadian Arctic," *Freshwater Biology*, vol. 47, no. 11, pp. 2123–2135, 2002.

[23] E. S. Al-Kharusi, D. E. Tenenbaum, and H. Abdi, "Large-scale Retrieval of Coloured Dissolved Organic Matter in Northern lakes using Sentinel-2 data[J]," *Remote Sensing*, vol. 12, p. 157, 2020.

[24] L. Wei, C. Huang, Z. Wang, Z. Wang, X. Zhou, and L. Cao, "Monitoring of Urban Black-Odor water based on Nemerow index and gradient Boosting Decision tree regression using UAV-Borne hyperspectral imagery," *Remote Sensing*, vol. 11, no. 20, p. 2402, 2019.

[25] C. C. Trees, P. W. Bissettb, M. A. Molined et al., "Monitoring water transparency and diver visibility in ports and harbors using aircraft hyperspectral remote sensing," in *Proceedings of the Photonics for Port and Harbor Security*, pp. 91–98, SPIE, Orlando, Florida, United States, May 2005.

[26] X. He, D. Pan, and Z. Mao, "Water-transparency (Secchi depth) monitoring in the China Sea with the SeaWiFS satellite sensor," in *Proceedings of the Remote Sensing for Agriculture, Ecosystems, and Hydrology VI*, pp. 55–68, SPIE, Maspalomas, Canary Islands, Spain, October 2004.

[27] N. B. Chang, S. Imen, and B. Vannah, "Remote sensing for monitoring Surface water quality Status and Ecosystem state in relation to the Nutrient Cycle: a 40-Year perspective," *Critical Reviews in Environmental Science and Technology*, vol. 45, no. 2, pp. 101–166, 2015.

[28] Z. P. Lee, S. Shang, C. Hu et al., "Secchi disk depth: a new theory and mechanistic model for underwater visibility," *Remote Sensing of Environment*, vol. 169, pp. 139–149, 2015.

[29] J. F. Knight and M. L Voth, "Application of MODIS imagery for intra-annual water clarity assessment of Minnesota lakes," *Remote Sensing*, vol. 4, no. 7, pp. 2181–2198, 2012.

[30] V. Pedroso Curtarelli, C. Clemente Faria Barbosa, D. Andrade Maciel et al., "Diffuse Attenuation of Clear water Tropical Reservoir: a remote sensing Semi-Analytical Approach," *Remote Sensing*, vol. 12, no. 17, p. 2828, 2020.

[31] G. Rodrigues, M. Potes, M. J. Costa et al., "Temporal and Spatial Variations of Secchi depth and Diffuse Attenuation coefficient from Sentinel-2 MSI over a large Reservoir," *Remote Sensing*, vol. 12, no. 5, p. 768, 2020.

[32] F. Setiawan, B. Matsushita, R. Hamzah, D. Jiang, and T Fukushima, "Long-Term Change of the Secchi disk depth in lake Maninjau, Indonesia Shown by Landsat TM and ETM+ data," *Remote Sensing*, vol. 11, no. 23, p. 2875, 2019.

[33] W. Yang, B. Matsushita, J. Chen, K. Yoshimura, and T Fukushima, "Retrieval of Inherent Optical Properties for Turbid Inland waters from remote-sensing reflectance," *IEEE Transactions on Geoscience and Remote Sensing*, vol. 51, no. 6, pp. 3761–3773, 2013.

[34] D. Brzezinski and J Stefanowski, "Reacting to Different types of Concept Drift: the accuracy Updated Ensemble algorithm," *IEEE Transactions on Neural Networks and Learning Systems*, vol. 25, no. 1, pp. 81–94, 2014.

[35] Y. Zhang, J. Ma, S. Liang, X. Li, and M. Li, "An evaluation of eight machine learning regression algorithms for forest Aboveground Biomass estimation from multiple satellite data Products," *Remote Sensing*, vol. 12, no. 24, p. 4015, 2020.

[36] D. Raspopov and P. Belousov, "Development of methods and algorithms for identification of a type of electric energy consumers using artificial intelligence and machine learning models for Smart Grid Systems," *Procedia Computer Science*, vol. 169, pp. 597–605, 2020.

[37] W. Wang and Y. Lu, "Analysis of the mean Absolute Error (MAE) and the Root mean Square Error (RMSE) in assessing Rounding model," *IOP Conference Series: Materials Science and Engineering*, vol. 324, Article ID 012049, 2018.

[38] J. Liu, Z. Yu, and D. Ma, "An adaptive fuzzy min-max neural network classifier based on principle component analysis and adaptive genetic algorithm," *Mathematical Problems in Engineering*, vol. 2012, pp. 1–21, 2012.

[39] L. Li, B. Lei, and C. Mao, "Digital Twin in Smart Manufacturing," *Journal of Industrial Information Integration*, vol. 26, no. 9, Article ID 100289, 2022.

[40] X. Xu and C. Wen, "Fault Diagnosis method based on information Entropy and relative principal component analysis," *Journal of Control Science and Engineering*, vol. 2017, Article ID 2697297, 2017.

[41] L. Li, T. Qu, Y. Liu et al., "Sustainability assessment of Intelligent Manufacturing supported by Digital Twin," *IEEE Access*, vol. 8, pp. 174988–175008, 2020.

[42] Y. Li, "Research and Implementation of Emotional classification of Traditional Folk Songs based on Joint time-Frequency analysis," *Mobile Information Systems*, vol. 2022, Article ID 1224274, 2022.

[43] L. Li and C. Mao, "Big data supported PSS evaluation Decision in Service-Oriented Manufacturing," *IEEE Access*, vol. 8, no. 99, pp. 154663–154670, 2020.

[44] Z. Xun, "Monitoring and analysis of English Classroom Teaching quality based on Big data," *Security and Communication Networks*, vol. 2022, Article ID 5365807, 2022.

[45] L. Li, C. Mao, H. Sun, Y. Yuan, and B. Lei, "Digital Twin Driven green Performance evaluation methodology of Intelligent Manufacturing: Hybrid model based on fuzzy rough-sets AHP, Multistage weight Synthesis, and PROMETHEE II," *Complexity*, vol. 2020, no. 6, pp. 1–24, 2020.

[46] J. Cai, J. Zhao, K. Shen, J. Liu, X. Li, and Y. Ye, "Exploring Factors Affecting the Yellow-Light Running Behavior of electric Bike Riders at Urban Intersections in China," *Journal of Advanced Transportation*, vol. 2020, Article ID 8573232, 2020.

[47] Y. Ai, H. Ma, Xu Qu, Y. Qian, Y. Liu, and W. Zhang, "The cross-Scale life prediction for the high-Speed Train Gearbox Shell based on the three-Interval method," *Scientific Programming*, vol. 2022, Article ID 6439229, 2022.

[48] H. Sun, F. Kong, C. Xiu, W. Shen, and Y. Wang, "A Progressive Combined variable selection method for Near-Infrared spectral analysis based on three-step Hybrid Strategy," *Journal of Spectroscopy*, vol. 2022, Article ID 2190893, 2022.

[49] L. Sun, M. Siddique, L. Wang, and S. J. Li, "Mixing characteristics of a bubble mixing microfluidic chip for genomic DNA extraction based on magnetophoresis: CFD simulation and experiment," *Electrophoresis*, vol. 42, no. 21-22, pp. 2365–2374, 2021.

[50] J. Tian, X. Chen, Z. Liang et al., "Application of NIR spectral Standardization based on principal component score evaluation in wheat Flour Crude Protein model Sharing," *Journal of Food Quality*, vol. 2022, Article ID 9009756, 2022.

[51] S. Cang and A. Wang, "Research on hyperspectral image Reconstruction based on GISMT Compressed sensing and Interspectral prediction," *International Journal of Optics*, vol. 2020, Article ID 7160390, 2020.